NUCLEAR SCIENCE AND ENGINEERING: **179**, 1–16 (2015)

Lumping Techniques for DFEM S_N Transport in Slab Geometry

Peter G. Maginot, Jean C. Ragusa,* and Jim E. Morel

Texas A&M University, Department of Nuclear Engineering
3133 TAMU, College Station, Texas 77843

Received August 14, 2013
Accepted May 5, 2014
http://dx.doi.org/10.13182/NSE13-65

Abstract—*We examine several mass matrix lumping techniques for the discrete ordinates (S_N) particle transport equations spatially discretized with arbitrary order discontinuous finite elements in one-dimensional (1-D) slab geometry. Though positive outflow angular flux is guaranteed with traditional mass matrix lumping for linear solution representations in source-free, purely absorbing 1-D slab geometry, we show that when used with higher-degree polynomial trial spaces, traditional lumping does not yield strictly positive outflows and does not increase the solution accuracy with increase in the polynomial degree of the trial space. As an alternative, we examine quadrature-based lumping strategies, which we term "self-lumping" (SL). Self-lumping creates diagonal mass matrices by using a numerical quadrature restricted to the Lagrange interpolatory points. When choosing equally spaced interpolatory points, SL is achieved through the use of closed Newton-Cotes formulas, resulting in strictly positive outflows for odd degree polynomial trial spaces in 1-D slab geometry. When selecting the interpolatory points to be the abscissas of a Gauss-Legendre or a Lobatto-Gauss-Legendre quadrature, it is possible to obtain solution representations with a strictly positive outflow in source-free pure absorber problems for any degree polynomial trial space in 1-D slab geometry. Furthermore, there is no inherent limit to local truncation error order of accuracy when using interpolatory points that correspond to Gauss-Legendre or Lobatto-Gauss-Legendre quadrature points.*

A single-cell analysis is performed to investigate outflow positivity and truncation error as a function of the trial space polynomial degree, the choice of interpolatory points, and the numerical integration strategy. We also verify that the single-cell local truncation error analysis translates into the expected global spatial convergence rates in multiple-cell problems.

I. INTRODUCTION

The linear discontinuous finite element method (LDFEM) for discrete ordinates radiation transport is widely used and has been extensively studied.[1–4] However, the discontinuous Galerkin finite element method (DFEM) does not limit solution approximations to linear trial spaces. Reed et al.[5] used arbitrary order DFEM S_N transport in TRIPLET, but because of data storage limitations at the time, only LDFEM was computationally practical. Possibly as a result of these historical computing limitations, the majority of reported DFEM radiation transport literature has focused on the LDFEM approximation. Higher-order DFEM methods have received periodic attention; some older examples include the work of Walters[6] and Hennart and del Valle.[7,8] More recent investigations of higher-order DFEM trial spaces include those of Warsa and Prinja[9] and Wang and Ragusa.[10,11] The primary focus of the work in Refs. 7 through 11 was the convergence rate of arbitrary order DFEM schemes.

Negative angular flux solutions obtained with LDFEM have been well documented in Refs. 2, 3, and 4. While these negativities do not affect the order of convergence and can be tolerated for certain applications,[12] some nonlinear problems, particularly radiative transfer calculations, can diverge if the angular intensities are negative. As a result, several methods to eliminate or inhibit negative solutions have been developed and can be categorized into one of three categories: ad hoc fix-ups,[2] strictly non-negative solution representations,[3] and matrix lumping.[4] The first two methods result in nonlinear systems of

*E-mail: jean.ragusa@tamu.edu

equations, while matrix lumping yields linear systems of equations. By definition, ad hoc fix-ups and strictly nonnegative solution representations yield nonnegative outflows in one-dimensional (1-D), two-dimensional, and three-dimensional geometries, regardless of material properties. Mass matrix lumping (applied to LDFEM) yields strictly positive outflows only in 1-D geometries, though it does otherwise inhibit negativities.[4] Although not related to DFEM discretizations, we note that other approaches have been investigated to mitigate negativities; see, for instance, Ref. 13.

Solution positivity of even degree unlumped DFEM methods for 1-D problems has been noted previously.[6–8] In comparing DFEM methods to nodal transport methods, Walters derived the quadratic DFEM scheme from the nodal transport equations using the Padé (2,3) approximation to the exponential term and noted that this approximation would result in a strictly positive outflow, regardless of cell optical thickness.[6] Hennart and del Valle then showed for slab geometry that all even P degree polynomial DFEM schemes approximate the cell outflow angular flux as a Padé $(P,P+1)$ function, which is a strictly positive approximation of the exponential.[7,8] The positivity of even degree unlumped DFEM for 1-D problems has also been shown in Ref. 9.

In this paper, we examine the idea of mass matrix lumping and its ability to ensure positive angular flux solutions for arbitrary degree DFEM trial spaces in nonscattering 1-D slab geometries. We consider traditional lumping (TL), which constructs a diagonal mass matrix by collapsing all off-diagonal entries onto the main diagonal,[4] and quadrature-based self-lumping (SL) methods,[14] which yield a diagonal mass matrix by numerically integrating the DFEM equations using the DFEM interpolatory points as quadrature points. Restricting ourselves to equally spaced interpolation points, SL numerical integration with the greatest degree of accuracy is achieved through the use of closed Newton-Cotes formulas.[15] However, Newton-Cotes formulas with a large number of integration points are known to be oscillatory and are of relatively low-order accuracy, integrating polynomials at most of degree equal to the number of integration points. By considering solution representations that employ quadrature points as the interpolatory points, for example, Gauss-Legendre (hereinafter Gauss) or Lobatto-Gauss-Legendre (hereinafter Lobatto) quadrature points,[15] we wish to find methods that are SL with a significantly higher accuracy. We analyze the following combinations of Lagrange interpolatory points and numerical integration strategies for positivity of the angular flux solution, local truncation error order, and spatial convergence order as a function of trial space polynomial degree:

1. exact numerical integration followed by collapsing the entries of the mass matrix onto the main diagonal (TL)
2. equally spaced interpolatory points and numerical integration via a Newton-Cotes formula at the interpolatory points
3. Gauss quadrature points as interpolatory points with numerical integration via a Gauss quadrature at the interpolatory points
4. Lobatto quadrature points as interpolatory points with numerical integration via a Lobatto quadrature at the interpolatory points
5. exact spatial integration.

We will use a shorthand name to refer to each of the above methods, as given in Table I. We limit the consideration of exact numerical integration schemes to those with equally spaced interpolatory points (exact integration with any particular set of interpolatory points will always yield the same DFEM solution).

It has long been noted that TL with equally spaced interpolatory points for 1-D LDFEM is equivalent to using the trapezoidal quadrature rule to approximately integrate the mass matrix[16] while exactly integrating the gradient operator. Since the trapezoidal rule is identical to the closed Newton-Cotes formula with two points, we hypothesize that for finite elements of arbitrary order using equally spaced interpolatory points, TL is equivalent to using a closed Newton-Cotes formula to compute the mass matrix while exactly integrating the gradient

TABLE I

Nomenclature of Numerical Schemes

Interpolation Point Type	Integration Strategy	Method Shorthand Name
Equally spaced	Exact spatial integration, with collapsing of mass matrix entries to the main diagonal	TL
Equally spaced	Numerical integration via Newton-Cotes quadrature restricted to interpolation points	SL Newton-Cotes
Gauss quadrature	Numerical integration via Gauss quadrature restricted to interpolation points	SL Gauss
Lobatto quadrature	Numerical integration via Lobatto quadrature restricted to interpolation points	SL Lobatto
Equally spaced	Exact spatial integration	Exact DFEM

operator. We demonstrate the equivalence between TL and closed Newton-Cotes formulas in the computation of the mass matrix.

Self-lumping based on Newton-Cotes formulas differs from TL in that SL Newton-Cotes generally does not exactly integrate the gradient operator. Coincidentally, the gradient operator is exactly integrated for linear/quadratic trial spaces using a 2-point/3-point Newton-Cotes formula, respectively. However, for higher-degree polynomial trial spaces, the corresponding Newton-Cotes formula does not exactly integrate the gradient operator.

Self-lumping based on either Gauss or Lobatto quadratures exactly integrates the gradient operator in 1-D slab geometry for all degrees of polynomial trial spaces; thus, there is no need to distinguish between exact integration and quadrature integration of the gradient operator for the SL Gauss and SL Lobatto schemes.

We divide the remainder of this paper as follows. In Sec. II, we provide the weak form for the 1-D S_N equations discretized with DFEM and define the different mass matrix lumping techniques. In Sec. III, we discuss the properties of different numerical quadratures as applied to the 1-D DFEM S_N equations. Numerical results demonstrating the robustness and accuracy of the different numerical schemes for various DFEM degrees are given in Sec. IV. Finally, we summarize our results and conclusions in Sec. V.

II. LUMPING TECHNIQUES FOR THE 1-D S_N TRANSPORT EQUATION WITH ARBITRARY ORDER DFEM

II.A. Weak Form Derivation

Consider the 1-D slab geometry S_N transport equation:

$$\mu_d \frac{d\psi_d}{dx} + \sigma_t \psi_d = Q_d \ , \tag{1}$$

where

ψ_d = angular flux $[1/(\mathrm{cm}^2\cdot\mathrm{s}\cdot\mathrm{sr})]$ in the μ_d direction (μ_d is the d'th-directional cosine relative to the x-axis)

σ_t = total interaction cross section (cm^{-1})

Q_d = fixed angular source in the direction of μ_d $[1/(\mathrm{cm}^3\cdot\mathrm{s}\cdot\mathrm{sr})]$.

In all that follows, we consider only nonscattering media (pure absorbers). The scalar flux ϕ $(\mathrm{n/cm}^2\cdot\mathrm{s})$ is defined as

$$\phi(x) = 2\pi \int_{-1}^{1} \psi(x,\mu_d) d\mu_d \ . \tag{2}$$

For simplicity, we derive the DFEM equations for a single-cell domain, with $x \in [x_L, x_R]$. A known angular flux $\psi_{in,d}$ is defined on the incoming face of the domain for all μ_d. For $\mu_d > 0$, $\psi_{in,d}$ is defined only at x_L and for $\mu_d < 0$, $\psi_{in,d}$ is defined at x_R. We begin our derivation by first transforming the physical geometry to a reference element, $s \in [-1, 1]$. This affine transformation is such that

$$x = \bar{x} + \frac{\Delta x}{2} s \tag{3a}$$

and

$$dx = \frac{\Delta x}{2} ds \tag{3b}$$

with $\bar{x} = \frac{x_L + x_R}{2}$ and $\Delta x = x_R - x_L$. We seek a numerical approximation to the true angular flux ψ_d using Lagrange polynomials of degree P:

$$\psi_d(s) \approx \tilde{\psi}_d(s) = \sum_{j=1}^{N_P} \psi_{j,d} B_j(s) \ , \tag{4}$$

where the $\sim$ denotes the numerical approximation. The basis functions B_j are the canonical Lagrange polynomials

$$B_j(s) = \prod_{\substack{k=1 \\ k \neq j}}^{N_P} \frac{s - s_k}{s_j - s_k} \ , \tag{5}$$

and $N_P = P + 1$. To determine the N_P unknown coefficients of Eq. (4), we follow a standard discontinuous Galerkin procedure, successively multiplying Eq. (1) by weight function B_i and integrating by parts, hence generating N_P moment equations ($1 \le i \le N_P$). We assume that the cross sections are constant per cell. Inserting our solution representation $\tilde{\psi}_d$, the i'th moment equation is given by

$$\mu_d \left[B_i(1)\tilde{\psi}_d(1) - B_i(-1)\tilde{\psi}_d(-1) - \int_{-1}^{1} \tilde{\psi}_d(s) \frac{dB_i}{ds} ds \right] + \frac{\Delta x \sigma_t}{2} \int_{-1}^{1} B_i(s)\tilde{\psi}_d(s) ds = \frac{\Delta x}{2} \int_{-1}^{1} B_i(s) Q_d(s) ds \ . \tag{6}$$

We now introduce the upwind approximation to define the angular flux at the cell edges. For $\mu_d > 0$ the angular flux at the cell interfaces is

$$\tilde{\psi}_d(-1) = \psi_{in,d} \tag{7a}$$

and

$$\tilde{\psi}_d(1) = \sum_{j=1}^{N_P} \psi_{j,d} B_j(1) \ . \tag{7b}$$

Similarly for $\mu_d<0$,

$$\tilde{\psi}_d(-1)=\sum_{j=1}^{N_P}\psi_{j,d}B_j(-1) \tag{8a}$$

and

$$\tilde{\psi}_d(1)=\psi_{in,d}\ . \tag{8b}$$

In Eqs. (7a) and (8b), $\psi_{in,d}$ is either the known angular flux outflow from the upwind cell or a boundary condition. Inserting the definition of $\tilde{\psi}_d(s)$, Eq. (6) becomes, for $\mu_d>0$,

$$\mu_d\left[B_i(1)\left(\sum_{j=1}^{N_P}\psi_{j,d}B_j(1)\right)-B_i(-1)\psi_{in,d}-\int_{-1}^{1}\left(\sum_{j=1}^{N_P}\psi_{j,d}B_j(s)\right)\frac{dB_i}{ds}ds\right]+\frac{\Delta x\sigma_t}{2}\int_{-1}^{1}B_i(s)\times\left(\sum_{j=1}^{N_P}\psi_{j,d}B_j(s)\right)ds=\frac{\Delta x}{2}\int_{-1}^{1}B_i(s)Q_d(s)ds\ , \tag{9}$$

and, for $\mu_d<0$,

$$\mu_d\left[B_i(1)\psi_{in,d}-B_i(-1)\left(\sum_{j=1}^{N_P}\psi_{j,d}B_j(-1)\right)-\int_{-1}^{1}\left(\sum_{j=1}^{N_P}\psi_{j,d}B_j(s)\right)\frac{dB_i}{ds}ds\right]+\frac{\Delta x\sigma_t}{2}\int_{-1}^{1}B_i(s)\times\left(\sum_{j=1}^{N_P}\psi_{j,d}B_j(s)\right)ds=\frac{\Delta x}{2}\int_{-1}^{1}B_i(s)Q_d(s)ds\ . \tag{10}$$

Considering all of the N_P moment equations at once, we can write both Eqs. (9) and (10) in a single matrix form:

$$\left(\mu_d\mathbf{G}+\frac{\sigma_t\Delta x}{2}\mathbf{M}\right)\vec{\psi}_d=\frac{\Delta x}{2}\vec{Q}_d+\mu_d\psi_{in,d}\vec{f}\ . \tag{11}$$

In Eq. (11) we have made use of the following definitions: The vector of unknowns is given by

$$\vec{\psi}_d=\left[\psi_{1,d}\ldots\psi_{N_P,d}\right]^T\ . \tag{12}$$

The mass matrix $\mathbf{M}$ is

$$\mathbf{M}_{ij}=\int_{-1}^{1}B_i(s)B_j(s)ds\ . \tag{13}$$

The fixed source moment vector $\vec{Q}_d$ is a column vector of length N_P:

$$\vec{Q}_{d,i}=\int_{-1}^{1}B_i(s)Q_d(s)ds\,. \tag{14}$$

And, $\vec{f}$ is a column vector of length N_P:

$$\vec{f}_i=\begin{cases}B_i(-1) & \text{for } \mu_d>0\\ -B_i(1) & \text{for } \mu_d<0\end{cases}\ . \tag{15}$$

Matrix $\mathbf{G}$ is an $N_P\times N_P$ matrix, which we refer to as the gradient operator. When $\mu_d>0$, $\mathbf{G}$ is given by

$$\mathbf{G}_{ij}=B_i(1)B_j(1)-\int_{-1}^{1}\frac{dB_i}{ds}B_j(s)ds\,. \tag{16a}$$

For $\mu_d<0$, $\mathbf{G}$ is

$$\mathbf{G}_{ij}=-B_i(-1)B_j(-1)-\int_{-1}^{1}\frac{dB_i}{ds}B_j(s)ds\,. \tag{16b}$$

When interpolatory points are not located at the cell interfaces (i.e., at $s=\pm1$), the following can be noted:

1. $\vec{f}$ has N_P nonzero entries.
2. $B_i(\pm1)B_j(\pm1)\neq0$ for all $i,j=1,\ldots,N_P$.

When a Lagrange interpolatory point exists on the cell edges, then $\vec{f}$ has only one nonzero entry, and the product $B_i(\pm1)B_j(\pm1)\neq0$ only when $i=j=N_P$ for $\mu_d>0$ or when $i=j=1$ for $\mu_d<0$, as is the case when equally spaced points or a Lobatto quadrature are used as interpolation points.

We evaluate the integrals of Eqs. (13) and (16) using a numerical quadrature. A method exactly integrates a quantity when the quadrature rule used to evaluate the integral is accurate for polynomials of degree equal to or greater than the polynomial degree of the integrand. In general, the matrices are dense, and their entries are computed as

$$\mathbf{M}_{ij}\approx\sum_{q=1}^{N_q}w_qB_i(s_q)B_j(s_q) \tag{17}$$

and

$$\mathbf{G}_{ij}\approx sg(\mu_d)B_i(sg(\mu_d))B_j(sg(\mu_d))-\sum_{q=1}^{N_q}w_q\left.\frac{dB_i}{ds}\right|_{s=s_q}B_j(s_q)\ , \tag{18}$$

where

N_q = number of quadrature points to be used

w_q = weights associated with quadrature points s_q

$sg(a)$ = sign function defined as

$$sg(a)=\begin{cases}+1 & \text{if } a>0\\ -1 & \text{if } a<0\end{cases}. \tag{19}$$

II.B. Traditional Lumping

The TL scheme replaces $\mathbf{M}$ with $\hat{\mathbf{M}}$, the latter being formed by collapsing row entries onto the main diagonal via the following formula[4]:

$$\hat{\mathbf{M}}_{ij}=\begin{cases}\sum_{j=1}^{N_P}\mathbf{M}_{ij} & \text{for } i=j\\ 0 & \text{otherwise}\end{cases}. \tag{20}$$

II.C. Quadrature-Based Lumping

An alternative method of mass matrix lumping restricts the quadrature points to the interpolatory points where

$$B_i(s_j)=\begin{cases}1 & \text{if } s_i=s_j\\ 0 & \text{otherwise}\end{cases},\quad i=1,\ldots,N_P, \tag{21}$$

and the quadrature integration of Eq. (17) reduces to

$$\mathbf{M}_{ij}=\begin{cases}w_i & i=j\\ 0 & \text{otherwise}\end{cases}. \tag{22}$$

As mentioned previously, we refer to the implicit lumping of Eq. (22) as SL. Self-lumping is a method to automatically generate a diagonal mass matrix. We note that SL does not imply that the quadrature formula inexactly integrates the mass matrix.

II.D. Source Moment Evaluation

Historically, when discussing lumping techniques, the focus has been on matrix lumping,[4] and little attention was paid to lumping source terms. For instance, we consider δ-shaped volumetric sources (i.e., equal to 0 everywhere except at one given point) as an example of a highly skewed volumetric source. In such a case, the evaluation of $\vec{Q}_d$ using quadrature-based SL schemes is an open question. Obviously, quadrature-based schemes cannot evaluate Eq. (14) for δ-sources. To address this, we expand the source on a Legendre polynomial basis:

$$\hat{S}_d(s)=\sum_{n=0}^{P}S_nP_n(s) \tag{23a}$$

with

$$S_n=\frac{2n+1}{2}\int_{-1}^{1}Q_d(s)P_n(s)ds \tag{23b}$$

and evaluate $\vec{Q}_d$ as follows:

$$\vec{Q}_{d,i}=\int_{-1}^{1}B_i(s)\hat{S}_d(s)ds. \tag{24}$$

Note that if the right side of Eq. (24) is exactly integrated, this is equivalent to exactly integrating Eq. (14).

III. QUADRATURE POINT SELECTION

We consider three different types of interpolatory points: equally spaced, Gauss quadrature, and Lobatto quadrature. On the $[-1,1]$ interval, the $N_P=P+1$ equally spaced interpolation points for a degree P polynomial trial space are

$$s_j=-1+(j-1)\frac{2}{P},\quad j=1,\ldots,N_P. \tag{25}$$

Self-lumping using equally spaced interpolation points requires numerical integration with closed Newton-Cotes quadrature formulas. The N_P weights w_j used for Newton-Cotes numerical integration at the interpolation points do not follow a concise pattern, so we refer the reader to Ref. 15. The Gauss quadrature points are the N_P roots of the Legendre polynomial $P_{N_P}(s)$ (Ref. 15). The corresponding weights are

$$w_j=\frac{2}{(1-s_j^2)}\left[P'_{N_P}(s_j)\right]^2. \tag{26}$$

Lobatto quadrature points have fixed endpoints, $s_1=-1$, $s_{N_P}=1$. The remaining N_P-2 points are the roots of $P'_{N_P-1}(s)$ (Ref. 15), with corresponding weights

$$w_j=\begin{cases}\dfrac{2}{N_P(N_P-1)} & j=1,\ j=N_P\\ \dfrac{2}{N_P(N_P-1)\left[P_{N_P-1}(s_j)\right]^2} & \text{otherwise}\end{cases}. \tag{27}$$

The highest polynomial degree a particular SL quadrature formula exactly integrates is given in Table II for Newton-Cotes, Gauss, and Lobatto quadratures. Also listed in Table II is the maximum polynomial degree of the integrands present in the gradient and mass matrices.

Since the accuracy of an $N_P=P+1$ point Gauss quadrature integration exceeds the polynomial degree of the $\mathbf{M}$ and $\mathbf{G}$ integrands for a trial space of degree P, using the SL Gauss scheme will strictly yield the same numerical solution as any DFEM scheme that exactly

TABLE II

Accuracy of SL Quadratures for Trial Spaces of Different Polynomial Degree P*

Polynomial Degree of $\tilde{\psi}$	$N_P = P+1$	Degree of **M** Integrand	Degree of **G** Integrand	Accuracy of Newton-Cotes	Accuracy of Gauss	Accuracy of Lobatto
1	2	2	1	1	3	1
2	3	4	3	3	5	3
3	4	6	5	3	7	5
4	5	8	7	5	9	7
5	6	10	9	5	11	9
P	$P+1$	$2P$	$2P-1$	Odd $\tilde{\psi}$: P Even $\tilde{\psi}$: $P+1$	$2P+1$	$2P-1$

*Each quadrature uses $N_P = P+1$ points.

integrates **M** and **G**. Thus, the SL Gauss scheme yields the same numerical solution as the Exact DFEM scheme.

For linear and quadratic trial spaces, SL methods using either Lobatto or equally spaced interpolation points will yield identical solutions. This is a direct result of the two- and three-point Lobatto quadrature formulas being identical to the two- and three-point closed Newton-Cotes quadratures. This equivalence does not hold for higher-degree polynomial trial spaces because the Lobatto quadrature points will no longer correspond to the equally spaced quadrature points.

By definition, TL uses equally spaced interpolation points and exactly integrates the gradient operator. For cellwise constant cross sections, TL is equivalent to a numerical integration scheme that

1. uses equally spaced interpolation points
2. integrates the gradient operator exactly
3. uses a Newton-Cotes quadrature restricted to the DFEM interpolation points to compute the mass matrix.

The third point can easily be demonstrated. Indeed, with TL, $\mathbf{M}_{ij}$ is exactly computed, and then, a row-sum operation is performed on the rows of **M**; thus, the entries of the diagonal mass matrix computed for TL are

$$\hat{\mathbf{M}}_{ii} = \sum_{j=1}^{N_P} \int_{-1}^{1} B_i(s)B_j(s)ds = \int_{-1}^{1} B_i(s)\left[\sum_{j=1}^{N_P} B_j(s)\right]ds$$

$$= \int_{-1}^{1} ds B_i(s) \qquad \forall i = 1, \ldots, N_P, \tag{28}$$

because $\sum_j^{N_P} B_j(s) = 1 \ \forall s \in [-1, +1]$ by definition. The integral $\int_{-1}^{1} ds B_i(s)$ is exactly integrated using a closed Newton-Cotes formula with $N_P = P+1$ points since $B_i(s)$ is a polynomial of degree P. Finally, when the B_i functions are defined using equally spaced points, the use of a closed Newton-Cotes formula with N_P points yields

$$\hat{\mathbf{M}}_{ii} = \int_{-1}^{1} ds\, B_i(s) = \sum_{q=1}^{N_P} w_q B_i(s_q) = w_i\ , \tag{29}$$

because $B_i(s_q) = \delta_{iq}$. Thus, the diagonal mass matrix computed using TL contains the closed Newton-Cotes weights as diagonal entries and is equivalent to approximating **M** using closed Newton-Cotes quadrature in Eq. (22). We also numerically verify this in Table III for polynomial degrees up to 4.

For linear and quadratic trial spaces, the two- and three-point Newton-Cotes quadrature formulas exactly integrate the gradient operator, as shown in Table II. Thus, for linear and quadratic trial spaces, schemes that use (a) equally spaced interpolation points and TL or (b) equally spaced interpolation points and SL numerical integration or (c) Lobatto quadrature points as interpolation points and SL numerical integration will yield identical solutions.

IV. NUMERICAL RESULTS

In this section, we present numerical results for two 1-D slab problems. For the first problem, we consider a source-free pure absorber with vacuum boundary conditions on the right, a known flux $\psi_{in,d}$ incident on the left face, and a spatially constant total cross section σ_t. The second problem consists of a slab with vacuum boundary conditions on both sides, no scattering, constant σ_t, and a fixed δ-source.

For $\mu_d > 0$, the numerical approximations to the angular flux near the cell inflow and outflow are as follows:

$$\tilde{\psi}_{in,d} = \sum_{j=1}^{N_P} \psi_{j,d} B_j(-1) \tag{30}$$

and

$$\tilde{\psi}_{out,d} = \sum_{j=1}^{N_P} \psi_{j,d} B_j(1)\ . \tag{31}$$

TABLE III

Equivalence of TL and Newton-Cotes Approximation of the Mass Matrix

P	Exact Integration of $\mathbf{M}$	Row Sum of $\mathbf{M}$	Newton-Cotes w with $P+1$ points
1	$\begin{bmatrix} \frac{2}{3} & \frac{1}{3} \\ \frac{1}{3} & \frac{2}{3} \end{bmatrix}$	$\begin{bmatrix} \frac{1}{1} \end{bmatrix}$	$\begin{bmatrix} \frac{1}{1} \end{bmatrix}$
2	$\begin{bmatrix} \frac{4}{15} & \frac{2}{15} & -\frac{1}{15} \\ \frac{2}{15} & \frac{16}{15} & \frac{1}{15} \\ -\frac{1}{15} & \frac{2}{15} & \frac{4}{15} \end{bmatrix}$	$\begin{bmatrix} \frac{1}{3} \\ \frac{4}{3} \\ \frac{1}{3} \end{bmatrix}$	$\begin{bmatrix} \frac{1}{3} \\ \frac{4}{3} \\ \frac{1}{3} \end{bmatrix}$
3	$\begin{bmatrix} \frac{16}{105} & \frac{38}{280} & -\frac{3}{70} & \frac{19}{840} \\ \frac{33}{280} & \frac{27}{35} & -\frac{27}{280} & -\frac{3}{70} \\ -\frac{3}{70} & -\frac{27}{280} & \frac{27}{35} & \frac{33}{280} \\ \frac{19}{840} & -\frac{3}{70} & \frac{38}{280} & \frac{16}{105} \end{bmatrix}$	$\begin{bmatrix} \frac{1}{4} \\ \frac{3}{4} \\ \frac{3}{4} \\ \frac{1}{4} \end{bmatrix}$	$\begin{bmatrix} \frac{1}{4} \\ \frac{3}{4} \\ \frac{3}{4} \\ \frac{1}{4} \end{bmatrix}$
4	$\begin{bmatrix} \frac{292}{2835} & \frac{296}{2835} & -\frac{58}{945} & \frac{8}{405} & -\frac{29}{2835} \\ \frac{296}{2835} & \frac{256}{405} & -\frac{128}{945} & \frac{256}{2835} & \frac{8}{405} \\ -\frac{58}{945} & -\frac{128}{945} & \frac{208}{315} & -\frac{128}{945} & -\frac{58}{945} \\ \frac{8}{405} & \frac{256}{2835} & -\frac{128}{945} & \frac{256}{405} & \frac{296}{2835} \\ -\frac{29}{2835} & \frac{8}{405} & -\frac{58}{945} & \frac{296}{2835} & \frac{292}{2835} \end{bmatrix}$	$\begin{bmatrix} \frac{7}{45} \\ \frac{32}{45} \\ \frac{4}{15} \\ \frac{32}{45} \\ \frac{7}{45} \end{bmatrix}$	$\begin{bmatrix} \frac{7}{45} \\ \frac{32}{45} \\ \frac{4}{15} \\ \frac{32}{45} \\ \frac{7}{45} \end{bmatrix}$

Regardless of the sign of μ_d, the numerical approximation to the cell average angular flux is defined as

$$\tilde{\psi}_{A,d} = \frac{1}{2}\sum_{j=1}^{N_P} w_j \psi_{j,d} \; . \tag{32}$$

We used the following quadrature weight normalization: $\sum_{j=1}^{N_P} w_j = 2$. In Eqs. (30), (31), and (32), $\psi_{j,d}$ are the components of $\vec{\psi}_d$, the numerical solution obtained by solving Eq. (11). Hence, the numerical angular flux solution of any of the previously discussed DFEM schemes can be obtained as a function of h, the number of mean free paths (mfp's) divided by μ_d:

$$h = \frac{\sigma_t \Delta x}{\mu_d} \; . \tag{33}$$

IV.A. Incident Flux Single-Cell Outflow Comparison

For the incident flux problem, the analytical solution of Eq. (1) is

$$\psi(x,\mu_d)=\begin{cases}\psi_{in,d}\exp\left[-\dfrac{\sigma_t(x-x_L)}{\mu_d}\right] & \text{for } \mu_d>0\\ 0 & \text{for } \mu_d<0\end{cases}. \quad (34)$$

The analytic angular flux outflow, $\psi_{out,d}=\psi(x_R,\mu_d)$, is given by

$$\psi_{out,d}=\psi_{in,d}\exp[-h]\ . \quad (35)$$

Similarly, the analytic average angular flux within the cell $\psi_{A,d}$ is

$$\psi_{A,d}=\frac{1}{\Delta x}\int_{x_L}^{x_R}\psi(x,\mu_d)dx=\frac{\psi_{in,d}}{h}(1-\exp[-h])\ . \quad (36)$$

The solution components are given by

$$\vec{\psi}_d=\psi_{in,d}\left(\mathbf{G}+\frac{h}{2}\mathbf{M}\right)^{-1}\vec{f}\ , \quad (37)$$

which allows us to compare the various choices of interpolatory points and numerical integration strategies solely as a function of h.

Figure 1 shows the numerically calculated cell outflow $\tilde{\psi}_{out,d}$ as a function of h for all methods considered. All methods converge to the analytical solution as $h\to 0$; thus, we have zoomed in the range where the methods visually differ (i.e., $h\geq 1$). We observe the following:

1. SL Gauss yields strictly positive outflows for even degree polynomial trial spaces.

2. SL Lobatto and SL Newton-Cotes yield strictly positive outflows for odd degree polynomial trial spaces.

3. TL yields strictly positive outflows only for a linear trial space.

We also numerically verify the remarks made in Sec. III; that is,

1. SL Gauss is equivalent to Exact DFEM.

2. SL Lobatto, SL Newton-Cotes, and TL are equivalent for linear and quadratic trial spaces.

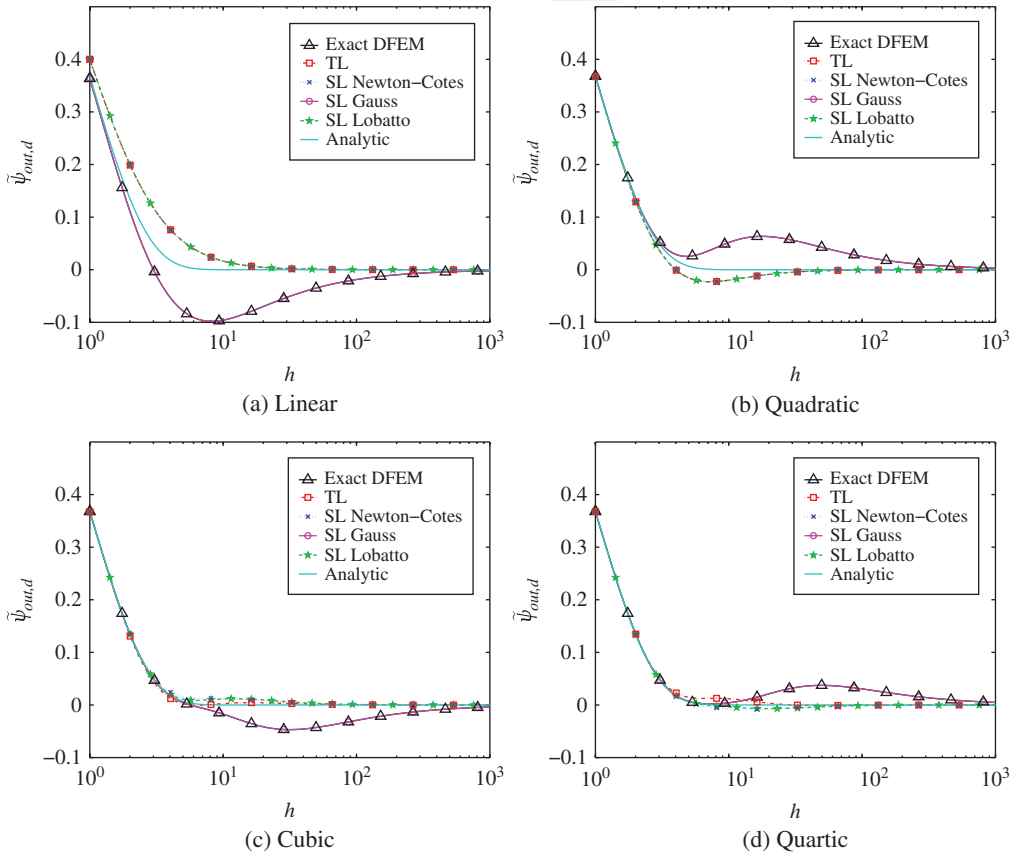

Fig. 1. Numerical outflow values as a function of h, $h=\sigma_t\Delta x/\mu$, for a single-cell homogeneous absorber problem employing polynomial orders $P=1$ through $P=4$.

3. For even degree trial spaces, the outflow value computed by SL Gauss is not monotonically decreasing as a function of h for cells of intermediate optical thickness (the same was noted in Ref. 9 for Exact DFEM).

IV.B. Fixed Source Single-Cell Inflow Comparison

As noted in Ref. 3, it is possible for LDFEM to yield negative solutions near cell inflows for source-driven problems. In this second problem, we use a δ-source:

$$Q_d(x)=\begin{cases}\delta(x-x_o) & \text{for } \mu_d>0\\ 0 & \text{for } \mu_d<0\end{cases}, \tag{38}$$

$x\in[-1,1]$, and $-1\le x_o\le 1$. The analytic solution to this problem for $\mu_d>0$ is

$$\psi(x,\mu_d)=\begin{cases}\exp\left[-\dfrac{\sigma_t(x-x_o)}{\mu_d}\right] & x\ge x_o\\ 0 & x<x_o\end{cases} \tag{39}$$

[for $\mu_d<0$, $\psi(x,\mu_d)=0$]. We now examine the numerical approximation to the angular flux near the cell inflow, $\tilde{\psi}_{in,d}$, for various integration schemes, for trial space degrees, and as a function of the ratio of the first Legendre moment of the source, S_1, to the zeroth Legendre moment of the source, S_0. Note that the physical range of that ratio $\frac{S_1}{S_0}$ is $[-3,3]$, corresponding to a δ-source at the left cell edge $\left(\frac{S_1}{S_0}=-3\right)$ or at the right edge $\left(\frac{S_1}{S_0}=3\right)$.

We first consider the case of a vacuum ($\sigma_t=0$), thus only testing the effect of quadrature accuracy in evaluating $\vec{Q}_d$ and **G**. In Fig. 2, we plot $\tilde{\psi}_{in,d}$ for three schemes:

1. Lobatto quadrature, which is exact for **G** and approximate for the source moments, Eq. (24)
2. Gauss quadrature, which is exact for both **G** and the source moments
3. Newton-Cotes quadrature, which is approximate for both **G** and the source moments.

The dotted vertical lines in Fig. 2 correspond to the extrema values of $\frac{S_1}{S_0}$ that yield a strictly positive polynomial source representation of degree P (indeed,

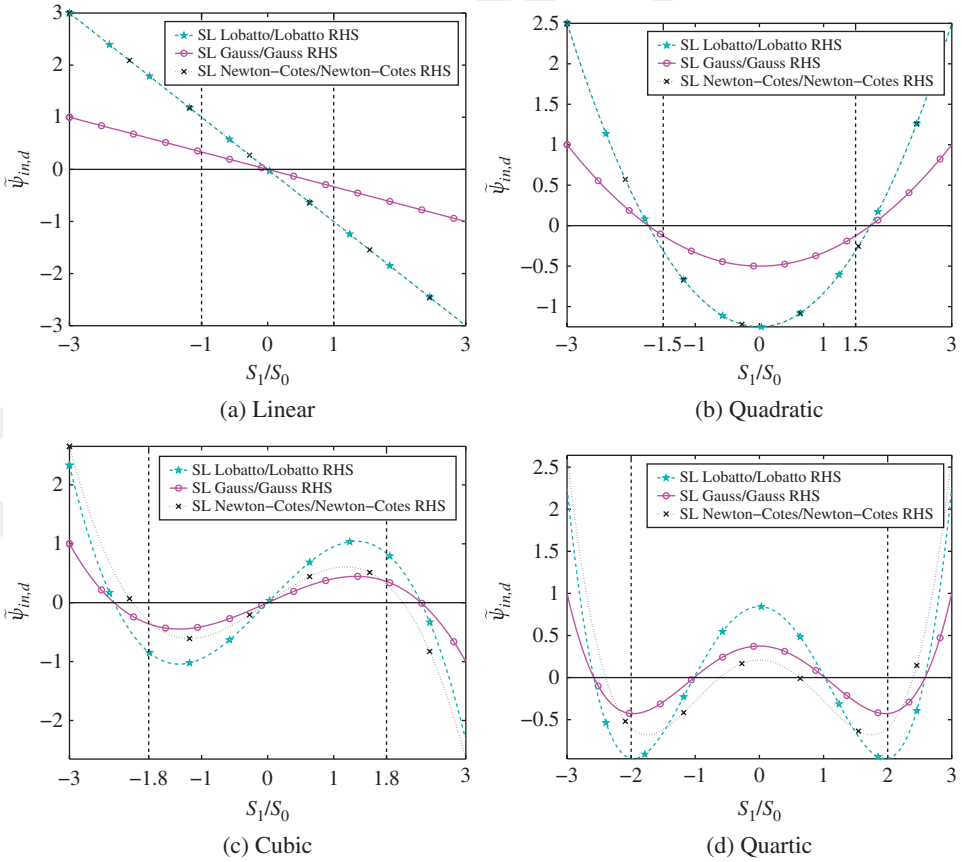

Fig. 2. Numerical inflow values as a function of $\frac{S_1}{S_0}$ for a single cell (vacuum case) with a δ-shaped source, using polynomial orders $P=1$ through $P=4$.

the degree-P Legendre expansion of the δ-source is not everywhere positive for a wide range of possible $\frac{S_1}{S_0}$ that are physically realizable). For all trial space degrees, the Gauss scheme exhibits less negativity than either of the other two schemes. The dramatic difference between the Gauss scheme and the Lobatto scheme is solely due to the quadrature formula used to evaluate $\vec{Q}_d$ since both schemes exactly integrate $\mathbf{G}$. The Newton-Cotes scheme exhibits less severe negativities than the Lobatto scheme but is less robust than the Gauss scheme. Given the results shown in Fig. 2, we conclude that the most robust schemes exactly integrate the source moments, Eq. (24).

In Fig. 3, we again examine the positivity of $\tilde{\psi}_{in,d}$, but for a nonvacuum case. The total cell optical thickness was chosen to be 5 mfp because this value led to the clearest plots. The relative behaviors observed do not change with cell optical thickness, but using a thicker domain reduces the magnitude for the values of $\tilde{\psi}_{in,d}$. All methods in Fig. 3 exactly integrate Eq. (24). Regardless of the trial space chosen, all schemes exhibit some negativities, but the SL Gauss scheme exhibits the greatest negativities and oscillations. The SL Newton-Cotes scheme presents the least severe negativities.

IV.C. Single-Cell Taylor Series Analysis

Next, we perform a local truncation error analysis by comparing the Taylor series expansions for the exact and numerical angular fluxes as a function of powers of h for the source-free, incident flux pure absorber problem. Matlab (Ref. 17) has been employed to perform the symbolic Taylor series expansions about $h=0$. We denote the Taylor-expanded quantities using the subscript T. The expansions for the analytical inflow, cell average, and outflow are as follows:

$$\psi_{in,d,T} = \psi_{in,d} \,, \tag{40a}$$

$$\psi_{A,d,T} = \psi_{in,d}\left(1-\frac{h}{2}+\frac{h^2}{6}-\frac{h^3}{24}+\frac{h^4}{120}-\frac{h^5}{720}\ldots\right) , \tag{40b}$$

and

$$\psi_{out,d,T} = \psi_{in,d}\left(1-h+\frac{h^2}{2}-\frac{h^3}{6}+\frac{h^4}{24}-\frac{h^5}{120}\ldots\right) . \tag{40c}$$

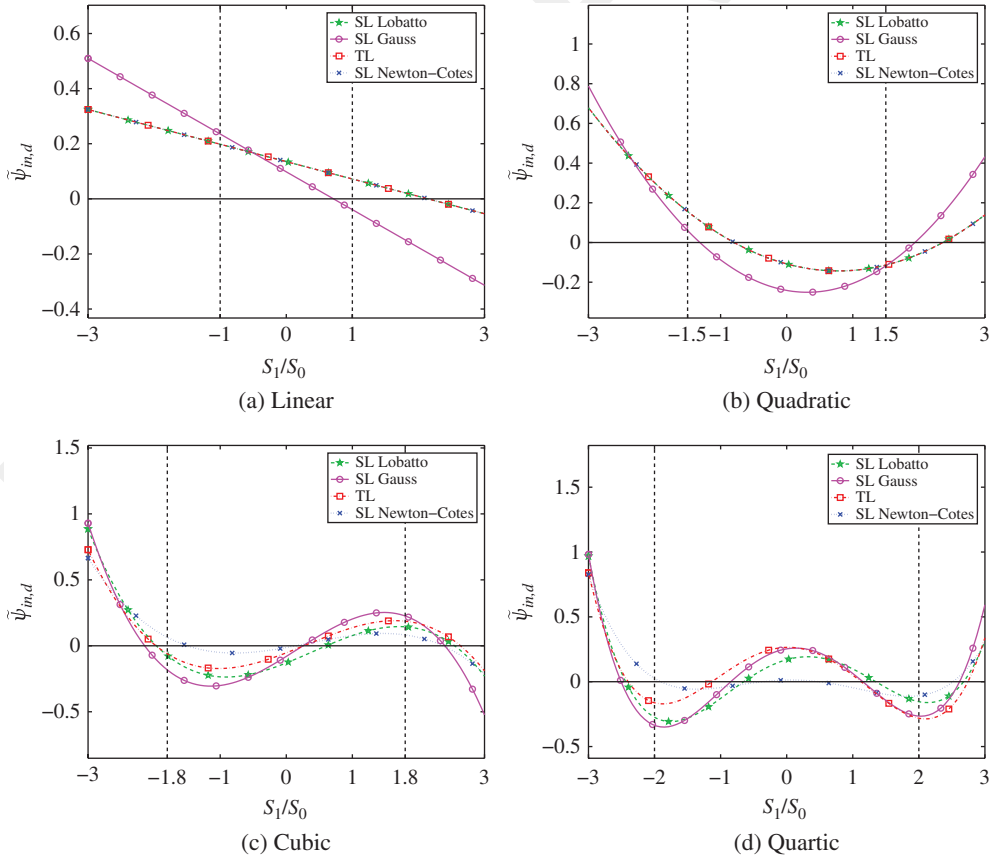

Fig. 3. Numerical inflow values as a function of $\frac{S_1}{S_0}$, for a single cell (absorber case) with a δ-shaped source, using polynomial orders $P=1$ through $P=4$.

The Taylor expansions of the numerical analogues to the quantities in Eqs. (40) depend on the trial space polynomial degree, the choice of interpolatory points, and the numerical integration strategy. For brevity, we omit giving these numerical analogues. Tables IV, V, and VI give the lowest-order h term and the magnitude of its constant (in parentheses) of the difference between the exact Taylor-expanded quantities and the corresponding

TABLE IV

Local Truncation Error Analysis in $\tilde{\psi}_{in,d}$ for a Single-Cell Problem with Constant Cross Section*

Polynomial Degree of $\tilde{\psi}$	Exact DFEM	TL	SL Newton-Cotes	SL Gauss	SL Lobatto
1	2 (2×10^{-1})	2 (5×10^{-1})	2 (5×10^{-1})	2 (2×10^{-1})	2 (5×10^{-1})
2	3 (2×10^{-2})	3 (4×10^{-2})	3 (4×10^{-2})	3 (2×10^{-2})	3 (4×10^{-2})
3	4 (1×10^{-3})	2 (7×10^{-2})	2 (1×10^{-1})	4 (1×10^{-3})	4 (3×10^{-3})
4	5 (7×10^{-5})	3 (1×10^{-2})	3 (1×10^{-2})	5 (7×10^{-5})	5 (1×10^{-4})
5	6 (3×10^{-6})	2 (5×10^{-2})	2 (6×10^{-2})	6 (3×10^{-6})	6 (7×10^{-6})
6	7 (1×10^{-7})	3 (1×10^{-2})	3 (9×10^{-3})	7 (1×10^{-7})	7 (3×10^{-7})
7	8 (4×10^{-9})	2 (5×10^{-2})	2 (4×10^{-2})	8 (4×10^{-9})	8 (8×10^{-9})

*Values given as $q(C)$ are to be read as Ch^q with $h=\sigma_t\Delta x/\mu$.

TABLE V

Local Truncation Error Analysis in $\tilde{\psi}_{A,d}$ for a Single-Cell Problem with Constant Cross Section*

Polynomial Degree of $\tilde{\psi}$	Exact DFEM	TL	SL Newton-Cotes	SL Gauss	SL Lobatto
1	3 (1×10^{-2})	2 (2×10^{-1})	2 (2×10^{-1})	3 (1×10^{-2})	2 (2×10^{-1})
2	5 (1×10^{-4})	4 (2×10^{-3})	4 (2×10^{-3})	5 (1×10^{-4})	4 (2×10^{-3})
3	7 (7×10^{-7})	3 (3×10^{-3})	4 (6×10^{-4})	7 (7×10^{-7})	6 (1×10^{-5})
4	9 (2×10^{-9})	5 (8×10^{-5})	6 (8×10^{-6})	9 (2×10^{-9})	8 (5×10^{-8})
5	11 (5×10^{-12})	3 (1×10^{-3})	6 (2×10^{-6})	11 (5×10^{-12})	10 (1×10^{-10})
6	13 (7×10^{-15})	5 (7×10^{-5})	8 (2×10^{-8})	13 (7×10^{-15})	12 (2×10^{-13})
7	Machine precision	3 (1×10^{-3})	8 (3×10^{-9})	Machine precision	Machine precision

*Values given as $q(C)$ are to be read as Ch^q with $h=\sigma_t\Delta x/\mu$. "Machine precision" entries are meant to indicate that Taylor series analysis was inconclusive due to all coefficients being within machine precision.

TABLE VI

Local Truncation Error Analysis in $\tilde{\psi}_{out,d}$ for a Single-Cell with Constant Cross Section*

Polynomial Degree of $\tilde{\psi}$	Exact DFEM	TL	SL Newton-Cotes	SL Gauss	SL Lobatto
1	4 (1×10^{-2})	3 (2×10^{-1})	3 (2×10^{-1})	4 (1×10^{-2})	3 (2×10^{-1})
2	6 (1×10^{-4})	5 (2×10^{-3})	5 (2×10^{-3})	6 (1×10^{-4})	5 (2×10^{-3})
3	8 (7×10^{-7})	4 (3×10^{-3})	5 (6×10^{-4})	8 (7×10^{-7})	7 (1×10^{-5})
4	10 (2×10^{-9})	6 (1×10^{-2})	7 (8×10^{-6})	10 (2×10^{-9})	9 (5×10^{-8})
5	12 (5×10^{-12})	4 (1×10^{-3})	7 (2×10^{-6})	12 (5×10^{-12})	11 (1×10^{-10})
6	14 (7×10^{-15})	6 (7×10^{-5})	9 (2×10^{-8})	14 (7×10^{-15})	13 (2×10^{-13})
7	Machine precision	4 (1×10^{-3})	9 (3×10^{-9})	Machine precision	Machine precision

*Values given as $q(C)$ are to be read as Ch^q with $h=\sigma_t\Delta x/\mu$. "Machine precision" entries are meant to indicate that Taylor series analysis was inconclusive due to all coefficients being within machine precision.

Taylor expansions of the numerical approximations to the angular flux near the cell inflow, cell average angular flux, and cell outflow angular flux, respectively. This local truncation error analysis illustrates the following:

1. Exact DFEM and SL Gauss, which are equivalent, exactly integrate the mass matrix and are the most accurate.

2. TL does not guarantee increasing order of accuracy by using higher-degree polynomial trial spaces.

3. TL converges at most third or fifth order for $\tilde{\psi}_{A,d}$ and fourth or sixth order for $\tilde{\psi}_{out,d}$ for odd or even polynomial trial spaces, respectively.

4. SL Newton-Cotes increases in accuracy with higher-degree polynomial trial spaces, but only for $\tilde{\psi}_{out,d}$ and $\tilde{\psi}_{A,d}$.

5. TL and SL Newton-Cotes are at most second order or third order accurate for $\tilde{\psi}_{in,d}$ for odd or even polynomial trial spaces, respectively.

6. SL Gauss is order $2P+1$ accurate in calculating $\tilde{\psi}_{A,d}$ and is order $2P+2$ accurate in calculating $\tilde{\psi}_{out,d}$.

7. SL Lobatto is order $2P$ accurate in calculating $\tilde{\psi}_{A,d}$ and is order $2P+1$ in calculating $\tilde{\psi}_{out,d}$.

8. SL Gauss, SL Lobatto, and Exact DFEM are accurate to order $P+1$ in calculating $\tilde{\psi}_{in,d}$.

9. SL Gauss is more accurate than SL Lobatto (smaller error constant) in computing $\tilde{\psi}_{in,d}$, but not an order of h.

IV.D. Convergence Rates for Spatially Discretized 1-D Domains

Here, we consider a homogeneous pure absorber material placed in a 1-D slab configuration and uniformly mesh the domain using N_{cells} cells. We use $x \in [0, 10\ \text{cm}]$, $\sigma_t = 1\ [\text{cm}^{-1}]$, no external sources, vacuum conditions on the right face of the slab, and a normally incident unit beam on the left face. The analytical solution to this problem is trivial to obtain:

$$\psi(x,\mu_d) = \begin{cases} \exp[-\sigma_t x] & \mu_d = 1 \\ 0 & \text{otherwise} \end{cases} . \quad (41)$$

The L_2 norm of the error is

$$E_\psi = \sqrt{\sum_{i=1}^{N_{cells}} \int_{x_{i-1/2}}^{x_{i+1/2}} \left(\psi(x,\mu_d) - \tilde{\psi}_{d,i}(x)\right)^2 dx}, \quad (42)$$

where we recall that $\tilde{\psi}_{d,i}(x)$ is the DFEM approximation of the angular flux in cell i. To evaluate the above integral, we use a high-order Gauss quadrature set $(x_{f,q}, w_{f,q})$ that employs a large number of quadrature points:

$$E_\psi \approx \sqrt{\sum_{i=1}^{N_{cells}} \frac{\Delta x_i}{2} \sum_{q=1}^{N_{qf}} w_{f,q} \left(\psi(x_{f,q},\mu_d) - \tilde{\psi}_d(x_{f,q})\right)^2} . \quad (43)$$

Values of E_ψ shown here are calculated using $N_{qf} = 10$. In addition to the L_2 error, we also present the cell average angular flux error E_{ψ_A}, defined as

$$E_{\psi_A} = \sqrt{\sum_{i=1}^{N_{cells}} \Delta x_i \left(\psi_{A,d,i} - \tilde{\psi}_{A,d,i}\right)^2}, \quad (44)$$

and the cell outflow error, $E_{\psi_{out}}$, given by

$$E_{\psi_{out}} = \sqrt{\sum_{i=1}^{N_{cells}} \Delta x_i \left(\psi(x_{i+1/2},\mu_d) - \tilde{\psi}_{out,d,i}\right)^2} . \quad (45)$$

In Eqs. (43), (44), and (45), Δx_i is the cell width of cell i, and $\psi_{A,d,i}$ is the exact cell-averaged angular flux in cell i, which, for $\mu_d = 1$, is simply

$$\psi_{A,d,i} = \exp[-\sigma_t x_{i-1/2}] \frac{1}{\sigma_t \Delta x_i} (1 - \exp[-\sigma_t \Delta x_i]) . \quad (46)$$

In Figs. 4, 5, and 6, we omit plotting the errors of Exact DFEM since the Exact DFEM solution is identical to that of SL Gauss. For linear and quadratic polynomials, we plot only SL Lobatto and omit plotting TL and SL Newton-Cotes since these methods yield identical solutions for linear and quadratic trial spaces. Figure 4 mirrors the results of Table IV, which is expected since the convergence rate of E_ψ will be limited by the slowest converging local approximation, which is $\tilde{\psi}_{in,d}$. Similarly, Fig. 5 is the multiple-cell analogue of the local truncation error analysis of $\tilde{\psi}_{A,d}$ given in Table V. As shown in Fig. 6, $E_{\psi_{out}}$ does not converge at the local truncation error rates of Table VI. The accumulation of errors in multiple-cell problems causes $E_{\psi_{out}}$ to globally converge one order of accuracy lower than the local truncation orders given in Table VI. It should be noted that the plateauing of errors E_ψ, E_{ψ_A}, and $E_{\psi_{out}}$ to values $\approx 10^{-14}$ in Figs. 4, 5, and 6, respectively, is simply a result of our numerical solutions being limited by machine precision (double precision).

V. CONCLUSIONS

Lumping methods for arbitrary order DFEM spatial discretizations of the first-order form of the S_N neutron transport equation have been studied in 1-D slab

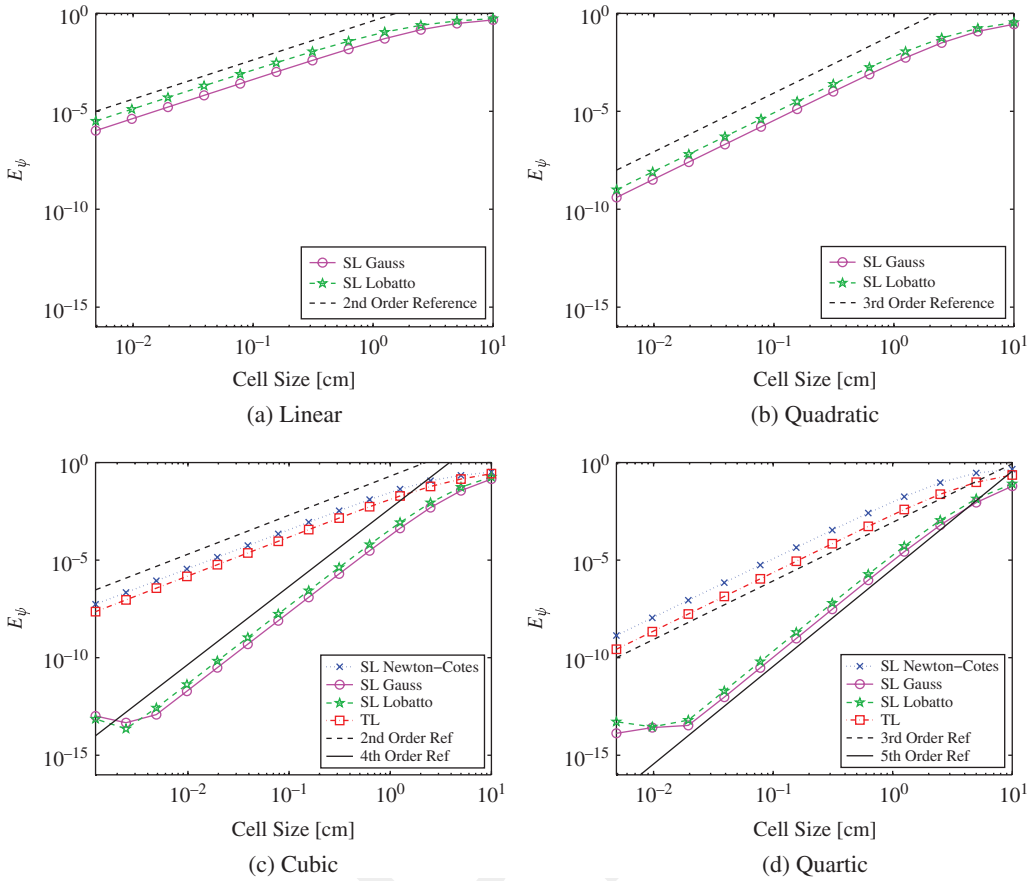

Fig. 4. Convergence rate of the L_2 norm of the error E_ψ as a function of the mesh cell size for a pure absorber $\{\sigma_t(x) = 1\ [\text{cm}^{-1}]$ and $x \in [0, 10\ [\text{cm}]]\}$.

geometry. We have analyzed lumping in terms of numerical integration strategy and finite element basis function interpolation point type. Accuracy and robustness of the various schemes have been assessed. Robustness is defined in the traditionally accepted assertion in the radiation transport community, i.e., resistance to negative outflow angular flux solutions in source-free pure absorbers with incident angular flux as cell optical thickness is increased. Two forms of mass matrix lumping were studied in an attempt to find DFEM discretization schemes that are both robust and yield higher-order accuracy with increases in the polynomial degree of the DFEM trial space.

The first scheme, traditional mass lumping or TL, exactly integrates the mass matrix and collapses row entries onto the main diagonal to create a diagonal mass matrix. Traditional lumping yields strictly positive angular flux outflows in a pure absorber with optically thick cells only when utilized with linear DFEM (LDFEM). The second form of mass matrix lumping considered here generates a diagonal mass matrix by restricting the DFEM interpolation points to the numerical quadrature points (this automatically generates a diagonal mass matrix). This SL concept may be new to the radiation transport community but was already presented in Refs. 14 and 16. in the general context of parabolic equations. We have extended these earlier works on SL quadratures by using arbitrary degree polynomial trial spaces and studied three types of interpolation points: (a) equally spaced points, (b) Gauss-Legendre quadrature, and (c) Lobatto-Gauss-Legendre quadrature. Using SL schemes, a strictly positive angular flux outflow can be obtained for all even degree polynomial trial spaces when employing Gauss-Legendre points (SL Gauss). Positive outflow is also obtained for all odd degree polynomial trial spaces using either equally spaced points (SL Newton-Cotes) or Lobatto-Gauss-Legendre quadratures (SL Lobatto). For source-driven problems, regardless of mass matrix lumping scheme, it is still possible to obtain negative angular fluxes near cell inflows, for certain source distributions.

In addition to the robustness of each scheme, we also considered the spatial convergence order of each method for a source-free purely absorbing medium with incident angular flux and constant cross section. The most accurate mass matrix lumping scheme was SL Gauss, for which the average and outflow angular fluxes converged with an

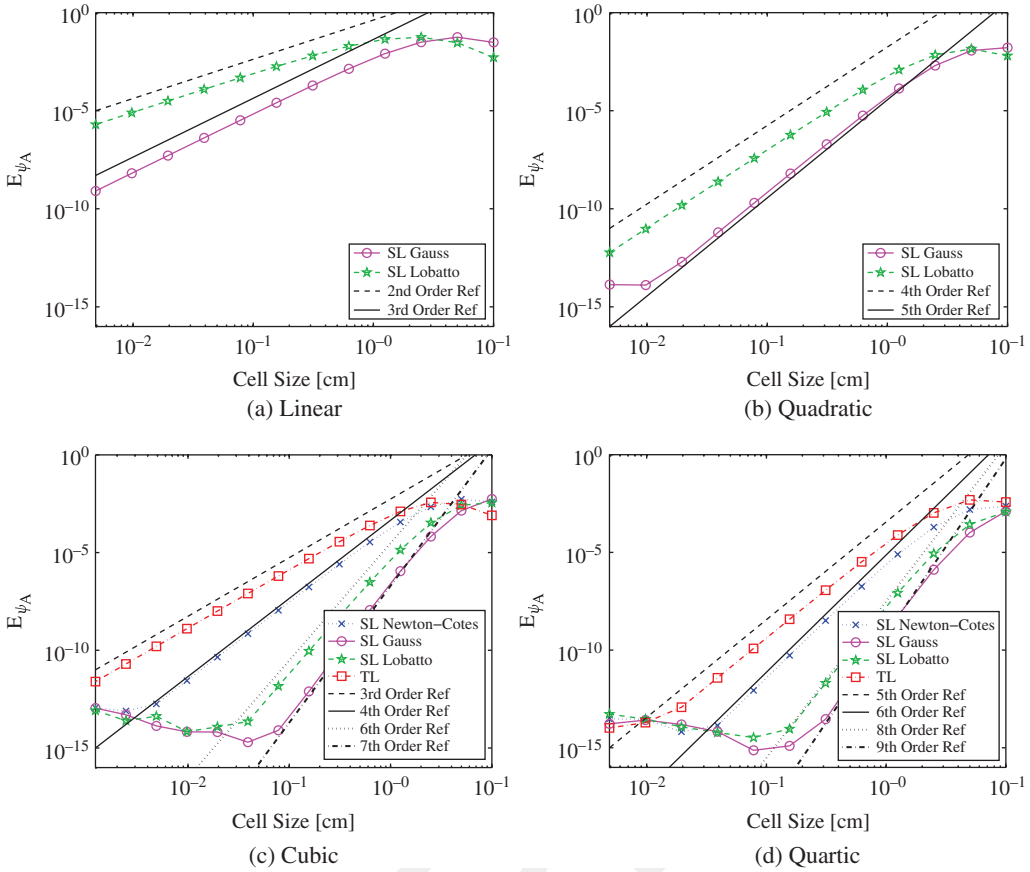

Fig. 5. Convergence rates for $E_{\psi,A}$ as a function of the mesh cell size for a pure absorber $\{\sigma_t(x) = 1\ [\text{cm}^{-1}]$ and $x \in [0, 10\ [\text{cm}]]\}$.

order $2P+1$, where P is the polynomial degree of the trial space employed. Since SL Gauss exactly integrates the mass matrix, its behavior is identical to employing exact DFEM, despite having a diagonal mass matrix. Traditional lumping was the least accurate of all schemes considered. Increasing the degree of the finite element trial space did not guarantee increased convergence order when using the TL scheme. The SL Newton-Cotes scheme performed better than TL; its order of convergence in the average and outflow angular fluxes increased with an increase in trial space polynomial degree, but in a suboptimal manner. Though not as accurate as SL Gauss for a given degree polynomial trial space, the SL Lobatto scheme only lagged the SL Gauss order of accuracy and spatial convergence by 1 for outflow and cell-averaged quantities.

In conclusion, we have shown that for arbitrary degree polynomial trial space DFEM, a diagonal mass matrix does not necessarily ensure strictly positive angular flux outflow in a purely absorbing slab with spatially constant cross section. Also, we have shown that by using quadrature-based lumping schemes and choosing DFEM interpolation points that are not equally spaced, robust, accurate polynomial DFEM schemes can be obtained. Based on the observed robustness, accuracy, and spatial convergence order results, we conclude that for applications requiring robust solution techniques, the SL Lobatto scheme with odd degree polynomial trial space DFEM be used to discretize the angular flux. If p-adaptivity is desired, software should be developed such that the ability to use either Lobatto (for odd trial space degrees) or Gauss (for even trial space degree) quadrature as the DFEM interpolation points is possible. However, given the nonmonotonic behavior of the outflow angular flux as a function of the cell optical thickness when employing the SL Gauss scheme with even degree trial spaces for under-resolved problems, using SL Lobatto with an odd degree trial space would seem to be more accurate than using SL Gauss, despite SL Gauss being more accurate in the asymptotic (fine mesh) limit.

We see additional opportunities for investigation. In particular, we plan on examining the robustness and accuracy of SL DFEM schemes for situations where the cross section is not cellwise constant. In radiative transfer, the opacity (analogue of a cross section) strongly depends on temperature, with temperature varying also within each mesh cell. Thus, opacity is an arbitrary, possibly rapidly, varying function of space. The behavior of SL DFEM schemes when cross section is a continuously varying function of space will be of interest in radiative transfer calculations and, as such, should be considered as a topic of research on that subject.

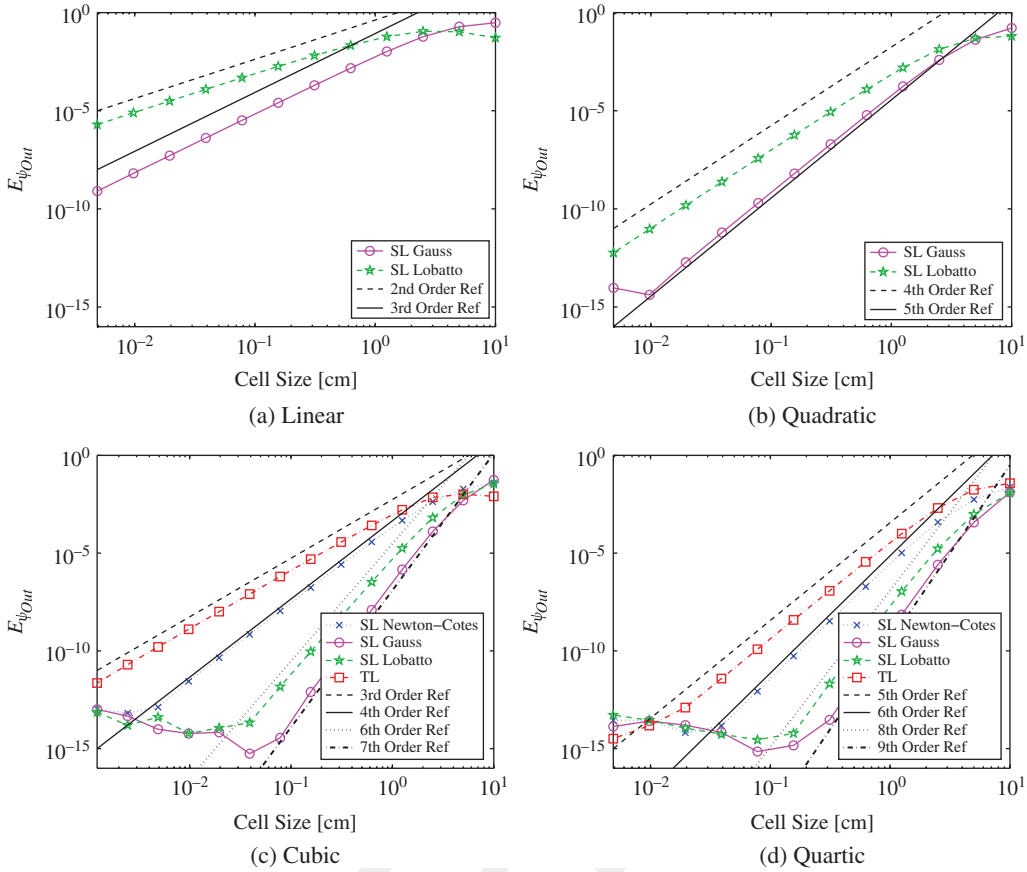

Fig. 6. Convergence rates for $E_{\psi,\,out}$ as a function of the mesh cell size for a pure absorber $\{\sigma_t(x) = 1\ [\mathrm{cm}^{-1}]$ and $x \in [0, 10\ [\mathrm{cm}]]\}$.

We also see opportunities to apply SL quadrature to multidimensional geometries. While we do not anticipate the multidimensional extensions of SL Lobatto or SL Gauss schemes to yield strictly positive angular flux outflows in multidimensional geometries, the mass matrix SL technique we have examined here in slab geometry provides a framework not only for mass matrix lumping but also for gradient matrix lumping. In multidimensional problems, mass matrix lumping alone has been shown to be insufficient in preventing solution oscillations. To reduce these oscillations, gradient operator lumping is also required.[4] Though gradient lumping is straightforward on orthogonal grids, it is an open topic of research for nonorthogonal grids.[18] Self-lumping methods may provide an adequate framework to carry out consistent mass and gradient lumping on nonorthogonal meshes.

ACKNOWLEDGMENTS

Portions of this work were made possible by the support of the U.S. Department of Energy (DOE) Computational Science Graduate Fellowship program, provided under DOE grant DE-FG02-97ER25308.

REFERENCES

1. E. W. LARSEN and W. F. MILLER, "Convergence Rates of Spatial Difference Equations for the Discrete-Ordinates Neutron Transport Equations in Slab Geometry," *Nucl. Sci. Eng.*, **73**, 76 (1980); http://dx.doi.org/10.13182/NSE80-3.

2. S. HAMILTON, M. BENZI, and J. WARSA, "Negative Flux Fixups in Discontinuous Finite Elements SN Transport," *Proc. Int. Conf. Mathematics, Computational Methods and Reactor Physics*, Saratoga Springs, New York, May 3–7, 2009, American Nuclear Society (2009).

3. P. MAGINOT, J. E. MOREL, and J. RAGUSA, "A Non-Negative Moment Preserving Spatial Discretization Scheme for the Linearized Boltzmann Transport Equation in 1-D and 2-D Cartesian Geometries," *J. Comput. Phys.*, **231,** *20*, 6801 (2012); http://dx.doi.org/10.1016/j.jcp.2012.06.018.

4. M. L. ADAMS, "Discontinuous Finite Element Transport Solutions in Thick Diffusive Problems," *Nucl. Sci. Eng.*, **137**, 298 (2001); http://dx.doi.org/10.13182/NSE00-41.

5. W. H. REED et al., "TRIPLET: A Two-Dimensional, Multigroup, Triangular Mesh, Planar Geometry, Explicit

Transport Code," LA-5428-MS, Los Alamos Scientific Laboratory (1973).

6. W. F. WALTERS, "The Relation Between Finite Element Methods and Nodal Methods in Transport Theory," *Prog. Nucl. Energy*, **18**, 21 (1986); http://dx.doi.org/10.1016/0149-1970(86)90009-0.

7. J. P. HENNART and E. DEL VALLE, "A Generalized Nodal Finite Element Formalism for Discrete Ordinate Equations in Slab Geometry: Part II: Theory in the Discontinuous Moment Case," *Transp. Theory Stat. Phys.*, **24**, 479 (1995); http://dx.doi.org/10.1080/00411459508206014.

8. J. P. HENNART and E. DEL VALLE, "A Generalized Nodal Finite Element Formalism for Discrete Ordinate Equations in Slab Geometry: Part III: Numerical Results," *Transp. Theory Stat. Phys.*, **24**, 505 (1995); http://dx.doi.org/10.1080/00411459508206015.

9. J. S. WARSA and A. K. PRINJA, "p-Adaptive Numerical Methods for Particle Transport," *Transp. Theory Stat. Phys.*, **28**, *3*, 229 (1999); http://dx.doi.org/10.1080/00411459908206036.

10. Y. WANG and J. C. RAGUSA, "On the Convergence of DGFEM Applied to the Discrete Ordinates Transport Equation for Structured and Unstructured Triangular Meshes," *Nucl. Sci. Eng.*, **163**, 56 (2009); http://dx.doi.org/10.13182/NSE08-72.

11. Y. WANG and J. C. RAGUSA, "A High-Order Discontinuous Galerkin Method for the SN Transport Equations on 2D Unstructured Triangular Meshes," *Ann. Nucl. Energy*, **36**, *7*, 931 (2009); http://dx.doi.org/10.1016/j.anucene.2009.03.002.

12. K. D. LATHROP, "Spatial Differencing of the Transport Equation: Positivity vs. Accuracy," *J. Comput. Phys.*, **4**, 475 (1969); http://dx.doi.org/10.1016/0021-9991(69)90015-1.

13. Y. AZMY, "Arbitrarily High Order Characteristic Methods for Solving the Neutron Transport Equation," *Ann. Nucl. Energy*, **19**, 593 (1992); http://dx.doi.org/10.1016/0306-4549(92)90004-U.

14. P. A. RAVIART, "The Use of Numerical Integration in Finite Element Methods for Solving Parabolic Equations," *Proc. Conf. Numerical Analysis (RIANA 1972)*, Dublin, Ireland, August 14–18, 1972, p. 233 (1972).

15. M. ABRAMOWITZ and I. A. STEGUN, *Handbook of Mathematical Functions with Formulas, Graphs, and Mathematical Tables*, U.S. Department of Commerce, Washington, D.C. (1972).

16. V. THOMEE, *Galerkin Finite Element Methods for Parabolic Problems*, Springer, New York (1997).

17. "MATLAB 2011b," The MathWorks (2011).

18. J. E. MOREL and J. S. WARSA, "Spatial Finite-Element Lumping Techniques for the Quadrilateral Mesh S_n Equations in *X-Y* Geometry," *Nucl. Sci. Eng.*, **156**, 325 (2007); http://dx.doi.org/10.13182/NSE06-13.